



# Probabilistic analysis and ghost-stochastic resonance of a hybrid energy harvester under Gaussian White noise

G. J. Fezeu · I. S. Mokem Fokou · C. Nono Dueyou Buckjohn · M. Siewe Siewe · C. Tchawoua

Received: 29 December 2019 / Accepted: 26 June 2020 / Published online: 16 July 2020  
© Springer Nature B.V. 2020

**Abstract** In this present work, a hybrid energy scavenger using two mechanisms of transduction namely piezoelectric and electromagnetic and subjected to the Gaussian white noise is investigated. The stochastic averaging method is used here in order to construct the Fokker–Plank–Kolmogorov equation of the system whose the statistic response in the stationary state is the probability density. The mean square voltage and current are obtained for different value of white noise intensities as the output power generated by piezoelectric circuit and electromagnetic circuit. In addition, combining the Gaussian white noise and coherence excitation, the Ghost-Stochastic resonance is observed through the mean residence time and improve the amount of energy harvested by the scavenger. The agreement between the analytical method and those obtained numerically validates the effectiveness of analytical investigations. The results obtained in this manuscript reveal that, while the natural frequency is absent in the external coherent

force, the amount of energy harvested by the energy scavenging device can be improved for certain value of noise intensity.

**Keywords** Probability · Mean residence time · Ghost-stochastic resonance

## 1 Introduction

Energy harvesting, known also as energy scavenging, covers a great body of technologies and devices that transform low grade energy sources such as solar energy, environmental vibrations, thermal energy, and human motion into usable electrical energy. Thanks to the recent technology progress recorded in the electronic domain, the electrical energy consumption by the electronics components has dramatically decreased, incited the proliferation of the wireless devices. Thus, the energy harvesting technology has become a very attractive solution for a wide variety of applications such as consumer electronics, outpatient medical electronics (hearing aids, pacemakers, smart implants) or imaging (camera inside the human body).

It is known in the literature that, there are three mechanisms allow to transduce vibration energy to electricity namely electrostatic [1], electromagnetic [2] and piezoelectric [3]. Many authors namely Elvin et al. [4], Inman [5], reviewing the state of the art on the energy harvesting. Most works on energy harvesting

---

G. J. Fezeu · I. S. M. Fokou (✉) · C. N. D. Buckjohn · M. S. Siewe · C. Tchawoua  
Faculty of science, Department of Physics, Laboratory of Mechanics, Materials and Structures, University of Yaounde I, P.O. Box: 812, Yaoundé, Cameroon  
e-mail: igormokem@yahoo.fr

I. S. M. Fokou  
The African Center of Excellence in Information and Communication Technologies (CETIC), Yaoundé, Cameroon

took the deterministic approach by considering the nonlinearity what can exhibit transduction materials and study its impact on the system performance. Mann [6] designed a nonlinear electromagnetic energy harvester that uses magnetic interactions to create a bistable potential well and validated the potential well escape phenomenon can be used to broaden the frequency response by theory and experiments. Spector et al. [7] proposed a theoretical model by using a beam element and performed experiment to harvest power from PZT material. They showed that a simple beam bending can provide the self-power source of the strain energy sensor. Kim et al. [8] reported that piezoelectric energy harvesting showed a promising results under pre-stress cyclic conditions and validated the experimental results with finite element analysis.

Let us notice that, the main objective in this research field is to enhance harvested energy by the devices. For this, build the hybrid system combining two mechanisms of transduction is essential. Bin et al. [9] built a hybrid energy harvester combined piezoelectric with electromagnetic mechanism to scavenge energy from external vibration. They studied the effect of the relative position of the coils and magnets on the PZT cantilever end and the poling direction of magnets on the output voltage of the harvested energy. Wang et al. [10] built a hybrid device for powering wireless sensor nodes in smart grid. It emerges from the results obtained that, from current-carrying conductor of 2.5 A at 50 Hz, the proposed harvester combining piezoelectric components and electromagnetic elements can generate up to 295.3  $\mu$ W. Madinei et al. [11] developed a hybrid cantilever beam harvester and by using an applied DC voltage as a control parameter to change the resonant frequency of the harvester to ensure resonance as the excitation frequency varies. These hybrid models mentioned above functioning in the surrounding where the vibration source can be modeled by the coherence excitation. However, in the most situations, the vibrations are random and time-varying. Cottone et al. [12] found numerically and experimentally that the nonlinear oscillators can outperform the linear ones under stochastic excitation. Fokou et al. [13] used a probabilistic approach to analytically predict the system's response, the stability and the estimation of system's reliability. Mokem et al. [14] proposed a hybrid device combining piezoelectric and electromagnetic transduction and subjected to the colored

noise. The authors shows that, the system performance can be improve for the small value of the relaxation time. Foupouapouognigni et al. [15] built the hybrid model and studied the stochastic resonance phenomenon, which is characterized by the large amplitude of vibration and increase the system performance. Let us remind that, when the nonlinear system is subjected to the combination of the harmonic excitation and the random force, many phenomena can be observed such as the stochastic resonance and the ghost-stochastic resonance. These two phenomena are characterized by the large amplitude of vibration. Indeed, the stochastic resonance occurs when the frequency of system's vibration is present in the frequency bandwidth of the harmonic excitation. However, when the maximum amplitude of the system is reached for a frequency of vibration absent in the frequency bandwidth of the harmonic force, this phenomenon is called a ghost-stochastic resonance.

While one observes in the literature, a growing interest in the theoretical investigation of the ghost-stochastic resonance phenomenon in the nonlinear systems [16–22], in our knowledge, the study of this phenomenon on the performance of the energy harvesting devices is not made. The main objective of this manuscript is to investigated the performance of the hybrid system when the ghost-stochastic resonance occurs (Fig. 1).

The rest of paper is organized as follows: In Sect. 2, we describe the system with model equation, followed by the assessment of the statistic response of the system. We draw the probability density function in

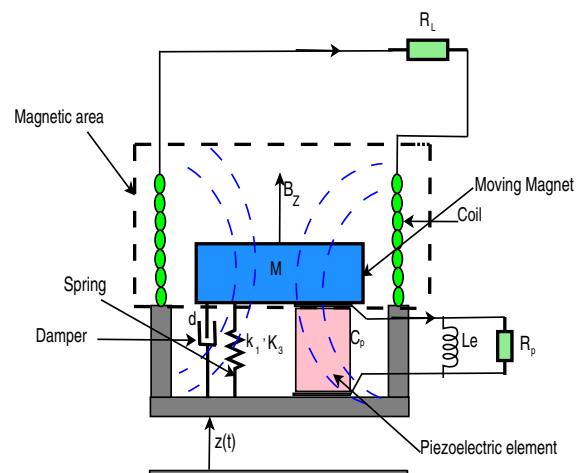


**Fig. 1** Schematic of the hybrid energy harvester

order to search for the probable amplitude of the mechanical and electrical response in Sect. 3. In Sect. 4, numerical simulations are made, from which we study the ghost-stochastic resonance. We conclude the Work in Sect. 5

## 2 Description of the system with the model equation

The design of hybrid energy harvester combining two mechanisms of transduction of ambient energy is composed of two parts namely the mechanical and the electrical part. We used the energy scavenger build by Lefeuvre in Ref.[23] with some modifications, by changing the rigid mass by a permanent magnet rod, and by adding a coil, in order to enhance the output power and enlarge its application field. It is worth noting that, in the schematic model, the mechanical part is composed of a nonlinear spring with the linear stiffness coefficient  $k_1$  and nonlinear stiffness coefficient  $k_3$  while the electrical part presents two subsystems namely the piezoelectric circuit and the electromagnetic circuit. The piezoelectric circuit is composed of the piezoelectric element and the load resistance  $R_p$ . The electromagnetic circuit has a permanent magnet of mass  $M$ , that produces a magnetic field  $B_z$ , the coil, connected to the rigid housing representing the stator is characterized by an inductance  $L_e$ . The load resistance of magnetic circuit is  $R_L$ . When the harvester is subjected to the external excitation  $Z(t)$ , the displacement of the magnetic mass  $M$  induces in the piezoelectric circuit, the deformation of piezoelectric element giving rise to the electrical field across the piezoelectric element. However, in the magnetic circuit, the displacement of the magnetic mass  $M$  induces a fluctuation of the magnetic flux in the surface of the coil, and consequently, a generation of electromotive force  $f_m(i) = B_z i L_{coil}$  in the mechanical part, while in the magnetic circuit, we can note the Lenz electromotive voltage  $f_e(z) = -B_z L_{coil} \dot{z}$  with  $z$ ,  $L_{coil}$ , and  $i$ , the displacement, the length of the coil and the current that flows in the coil respectively,  $B_z$  being the magnetic field generated by the permanent magnet. A summary of equations is provided here [23] giving a full derivation of the mechanical and piezoelectric circuit equations. Using the Kirchhoff’s law in the

electromagnetic circuit by letting  $\mathbf{B}_z = B\mathbf{u}_z$ , we obtained motion equations given by:

$$\begin{aligned}
 M\ddot{z} + d\dot{z} + k_1z + k_3z^3 + Bil_{coil} - \theta_2 v &= Z(t) \\
 C_p\dot{v} + \frac{v(t)}{R_p} + \theta_2\dot{z} &= 0 \\
 L_e\dot{i} + R_Li - Bl_{coil}\dot{z} &= 0
 \end{aligned}
 \tag{1}$$

where  $d$  is the damping coefficient,  $C_p$ , the capacity of the capacitor and  $\theta_2$  the electromechanical coupling coefficient. The physical parameters used in this manuscript are given in Table 1.

By using the time-transformation ( $t = \frac{\tau}{\omega}$ ), Eq. (1) gives rise to the following non-dimensional system:

$$\begin{aligned}
 x'' + \mu a x' + \omega_0 x - \beta_2 y + \sigma x^3 + \beta_1 r &= N(\tau)(a) \\
 y' + \alpha_2 y - \beta_{22} x' &= 0(b) \\
 r' + \alpha_3 r - \beta_{11} x' &= 0(c)
 \end{aligned}
 \tag{2}$$

with  $N(\tau) = \sum_{i=1}^m f_0 \cos(\omega_i \tau) + \xi(\tau)$  where  $\sum_{i=1}^m f_0 \cos(\omega_i \tau)$  is a harmonic excitation, with  $f_0$  the amplitude of coherence force,  $\omega_i = (k + i - 1)\omega_0$  is the frequency of the coherence force with  $k$  a constant took here equal to 2.  $\omega_0$  is the fundamental frequency. The variable  $\xi(\tau)$ , is the Gaussian white noise verifying the statistics properties:  $\langle \xi(\tau) \rangle = 0$ ,

**Table 1** Physical parameters of hybrid model

Parameter	Value	Unit
$L_{coil}$	0.03	$m$
$M$	1	$mg$
$k_1$	-100	$N/m$
$k_3$	500	$N/m$
$d$	0.1	-
$\theta_2$	0.1	-
$R_L$	1	$k\Omega$
$B$	0.1	$T$
$L_e$	1	$mH$
$C_p$	4	$F$
$R_p$	500	$\Omega$

$\langle \xi(\tau)\xi(s) \rangle = 2D\delta(\tau)$ . The dimensionless parameters are given as follow:

$$\mu_a = -\frac{\omega d}{k_1}; \sigma = -\frac{l^2 k_3}{k_1}; \beta_2 = -\frac{\theta_2 v_o}{lk_1}; \beta_1 = -\frac{BL_{coil} i_o}{lk_1}$$

$$\alpha_2 = \frac{1}{\omega C_p R_p}; \beta_{22} = -\frac{\theta_2 l}{v_o C_p}; \beta_{11} = \frac{IBL_{coil}}{Li_o}; \alpha_3 = \frac{R_L}{\omega L_e};$$

$$z = lx(\tau\omega); v = v_o y(\tau\omega); i = i_o r(\tau\omega);$$

$$N(\tau) = -Z\left(\frac{\tau}{\omega}\right)l^{-1}k_1^{-1} \tag{3}$$

### 3 Stochastic averaging method

In this heading, we assume that,  $f_0 = 0$ . We use the stochastic averaging method to provide the statistic response of the harvester. In the quasi-harmonic regime, the solution of the mechanical system (2) is of the form:

$$x(\tau) = a(\tau)(\tau) \cos(\theta); \quad x'(\tau) = -\omega a(\tau)(\tau) \sin(\theta) \tag{4}$$

where  $\theta = \omega\tau + \psi(\tau)$  with  $\psi$ , the phase angle and  $a(\tau)$  the amplitude. Substituting Eq. (4) into Eq. (2) (b)–(c), the solution of obtained equation can be written as follow:

$$y(\tau) = C_1 e^{-\alpha_2 \tau} + \frac{\beta_{22} a(\tau) \omega (\omega \cos(\theta) - \alpha_2 \sin(\theta))}{\omega^2 + \alpha_2^2}$$

$$r(\tau) = C_2 e^{-\alpha_3 \tau} + \frac{a(\tau) \beta_{11} \omega (\omega \cos(\theta) - \alpha_3 \sin(\theta))}{\omega^2 + \alpha_3^2} \tag{5}$$

In the steady state, Eqs. (5 a)–(b) can be rewritten as:

$$y(\tau) = \frac{\beta_{22} a(\tau) \omega (\omega \cos(\theta) - \alpha_2 \sin(\theta))}{\omega^2 + \alpha_2^2}$$

$$r(\tau) = \frac{a(\tau) \beta_{11} \omega (\omega \cos(\theta) - \alpha_3 \sin(\theta))}{\omega^2 + \alpha_3^2} \tag{6}$$

where

$$\omega \cos(\theta) - \alpha_2 \sin(\theta) = \sqrt{\omega^2 + \alpha_2^2} \cos\left(\theta + \arctan\left(\frac{\alpha_2}{\omega}\right)\right)$$

$$\omega \cos(\theta) - \alpha_3 \sin(\theta) = \sqrt{\omega^2 + \alpha_3^2} \cos\left(\theta + \arctan\left(\frac{\alpha_3}{\omega}\right)\right) \tag{7}$$

Thus, the amplitudes of steady-state current and charge are given by:

$$Y = \frac{\beta_{22} a \omega}{\sqrt{\omega^2 + \alpha_2^2}}; R = \frac{a \beta_{11} \omega}{\sqrt{\omega^2 + \alpha_3^2}} \tag{8}$$

Substituting Eqs. (4) and (6) into Eq. (2), and applying the determinist averaging method in the determinist part of the obtained system, we have:

$$a' = -\frac{\gamma_{22} N(\tau) \sin(\theta)}{2\omega \gamma_{55}} - \frac{\gamma_{11} a}{2\omega \gamma_{55}} \tag{9}$$

$$\phi' = \frac{\gamma_{33} N(\tau) \cos(\theta)}{\gamma_{44} a} + \frac{a^2 \gamma_{12}}{\gamma_{44}} + \frac{\gamma_{13}}{\gamma_{44} a}$$

where

$$\gamma_{11} = \beta_1^2 \omega^3 \alpha_3 - \beta_2^2 \omega^3 \alpha_2 + \mu_a \omega^3 \alpha_3^2 + \mu_a \omega^5$$

$$+ \mu_a \omega \alpha_2^2 \alpha_3^2 + \mu_a \omega^3 \alpha_2^2 - \beta_2^2 \omega \alpha_2 \alpha_3^2 + \beta_1^2 \omega \alpha_3 \alpha_2^2$$

$$\gamma_{22} = 2 \alpha_2^2 \omega^2 + 2 \alpha_2^2 \alpha_3^2 + 2 \omega^2 \alpha_3^2 + 2 \omega^4$$

$$\gamma_{33} = -8 \alpha_2^2 \alpha_3^2 - 8 \omega^4 - 8 \omega^2 \alpha_3^2 - 8 \alpha_2^2 \omega^2$$

$$\gamma_{44} = 8 \omega^5 + 8 \omega^3 \alpha_3^2 + 8 \omega^3 \alpha_2^2 + 8 \omega \alpha_2^2 \alpha_3^2$$

$$\gamma_{55} = \omega^4 + \omega^2 \alpha_3^2 + \alpha_2^2 \omega^2 + \alpha_2^2 \alpha_3^2$$

$$\gamma_{12} = 3 \sigma \omega^2 \alpha_3^2 + 3 \sigma \alpha_2^2 \omega^2 + 3 \sigma \omega^4 + 3 \sigma \alpha_2^2 \alpha_3^2$$

$$\gamma_{13} = -4 \omega^2 \alpha_2^2 \alpha_3^2 + 4 \beta_1^2 \omega^4 - 4 \omega^4 \alpha_2^2 - 4 \omega^6 - 4 \beta_2^2 \omega^4$$

$$-4 \omega^4 \alpha_3^2 + 4 \beta_1^2 \omega^2 \alpha_2^2 - 4 \beta_2^2 \omega^2 \alpha_3^2$$

$$+ 4 \omega_0 \alpha_2^2 \alpha_3^2 + 4 \omega_0 \alpha_2^2 \omega^2 + 4 \omega_0 \omega^2 \alpha_3^2 + 4 \omega_0 \omega^4 \tag{10}$$

Finally, applying the stochastic averaging method, in Eq. (9), we obtain the Ito equation defined as:

$$da = \left( -\frac{2\gamma_{11}a}{\omega\gamma_{55}} + \frac{D}{2a\omega^2} \right) dt + \sqrt{\frac{D}{\omega^2}} dB_1$$

$$d\theta = \frac{(\gamma_{12}a^2 + \gamma_{13})dt}{\gamma_{44}} + \sqrt{\frac{D}{\omega^2 a^2}} dB_2$$
(11)

where  $B_1$  and  $B_2$  are the normalized wiener process. We observe in Eq. (11) that  $a$  and  $\theta$  are independent. Thus, we can provided the probability density for the amplitudes(  $a$ ), rather than a joint probability density for  $\theta$ . The probability density  $P(a, \tau)$  of the instantaneous amplitude  $a$  satisfies the Fokker–Planck–Kolmogorov equation:

$$\frac{\partial}{\partial \tau} p(a, \tau) = -\left( -\frac{\gamma_{11}}{2\omega\gamma_{55}} - \frac{D}{\omega^2 2a^2} \right) p(a, \tau)$$

$$-\left( -\frac{\gamma_{11}a}{2\omega\gamma_{55}} + \frac{D}{2a\omega^2} \right) \frac{\partial}{\partial a} p(a, \tau) + \frac{(D)\frac{\partial^2}{\partial a^2} p(a, \tau)}{2\omega^2}$$
(12)

In the stationary state, the solutions of Eq. (12) is given by:

$$p(a) = Nae^{-\frac{\gamma_{11}a^2\omega}{(2D)(\omega^2+\alpha_3^2)(\omega^2+\alpha_2^2)}} \tag{13}$$

where  $N$  is the normalization constant which can be assessed numerically using Simpson’s method. Through a transformation from variable  $(a, \theta)$ , to the original variables  $(x, x')$ , an expression for the stationary densities function of  $x$  and  $x'$  can be derived as:

$$P_n(x, x') = \frac{P(a, \theta)}{2\pi a} \tag{14}$$

$$p(a) = \frac{N}{2\pi} \exp\left( -\frac{\gamma_{11}\omega\left(x^2 + \frac{x'^2}{\omega^2}\right)}{2D(\omega^2 + \alpha_3^2)(\omega^2 + \alpha_2^2)} \right) \tag{15}$$

Thus, the expected value of the mean square electric current and charge can be calculated following this formula (Fig. 3):

$$\langle y^2(\tau) \rangle = \langle Y^2 \rangle = \left( \frac{\beta_{22}\omega}{\sqrt{\omega^2 + \alpha_2^2}} \right)^2 \times \langle a^2 \rangle$$

$$= \left( \frac{\beta_{22}\omega}{\sqrt{\omega^2 + \alpha_2^2}} \right)^2 \int_0^{+\infty} a^2 p(a) da$$

$$\langle Y^2 \rangle = \frac{2\beta_{22}^2\omega D(\omega^4 + \omega^2(\alpha_3^2 + \alpha_2^2) + \alpha_2^2\alpha_3^2)}{\gamma_{11}(\omega^2 + \alpha_2^2)}$$
(16)

and

$$\langle r^2(\tau) \rangle = \langle R^2 \rangle = \left( \frac{\beta_{11}\omega}{\sqrt{\omega^2 + \alpha_2^2}} \right)^2 \times \langle a^2 \rangle$$

$$= \left( \frac{\beta_{11}\omega}{\sqrt{\omega^2 + \alpha_3^2}} \right)^2 \int_0^{+\infty} a^2 p(a) da$$

$$\langle R^2 \rangle = \frac{2\beta_{11}^2\omega D(\omega^4 + \omega^2(\alpha_3^2 + \alpha_2^2) + \alpha_2^2\alpha_3^2)}{\gamma_{11}(\omega^2 + \alpha_3^2)}$$
(17)

### 4 Numerical simulation

#### 4.1 Algorithm of numerical simulation

The numerical scheme used in this manuscript is based on the Euler version algorithm. By letting  $\dot{x} = u$ , Eq. (2) can be rewritten as follow:

$$x' = u$$

$$u' = -\mu_a u - \omega_0 x + \beta_2 y - \sigma x^3 - \beta_1 r + N(\tau)$$

$$y' = -\alpha_2 y + \beta_{22} u$$

$$r' = -\alpha_3 y + \beta_{11} u$$
(18)

The discrete equations can be written as:

$$x_{i+1} = x_i + u_i h$$

$$u_{i+1} = u_i + [-\mu_a u_i - \omega_0 x_i + \beta_2 y_i - \sigma x_i^3 - \beta_1 r_i] h + \zeta_k(\tau)$$

$$y_{i+1} = y_i + [-\alpha_2 y_i + \beta_{22} u_i] h$$

$$r_{i+1} = r_i + [-\alpha_3 y_i + \beta_{11} u_i] h$$
(19)

In the purpose to compare the analytical results obtained via the stochastic averaging method, the numerical simulation is made for the harvester.

Figure 4, shows the good agreement between the numerical results and those obtained analytically. We also draw in Fig. 2, the 3D representation of probability density of harvester. It emerges from these results that, the probability distribution is unimodal.

#### 4.2 Mean residence time and ghost-stochastic resonance phenomenon

In this heading, we assume that,  $f_0 \neq 0$ . Thus, the harvester is subjected to the combination of the coherence excitation  $\sum_{i=1}^m f_0 \cos(\omega_i \tau)$  and the random force  $\zeta_k(\tau)$ . In the purpose to get a deep understanding

of the observed dynamics and the influence of noise, we can assess the mean residence time and mean amplitude response.

Let us remind that equation(Eq.(2)) is nonlinear and should exhibit many frequency components. For the large value of time( $\tau \rightarrow \infty$ ), the asymptotic solution of Eq.(2) can be given as follows:

$$\langle x(\tau) \rangle_{as} = \sum_j x_m(j\omega_i) \cos[j\omega_i \tau - \psi_m(j\omega_i)] \tag{20}$$

where  $j$  is a non-negative constant which may be in integer or fractional form,  $x_m(j\omega_i)$  and  $\psi_m(j\omega_i)$  are the

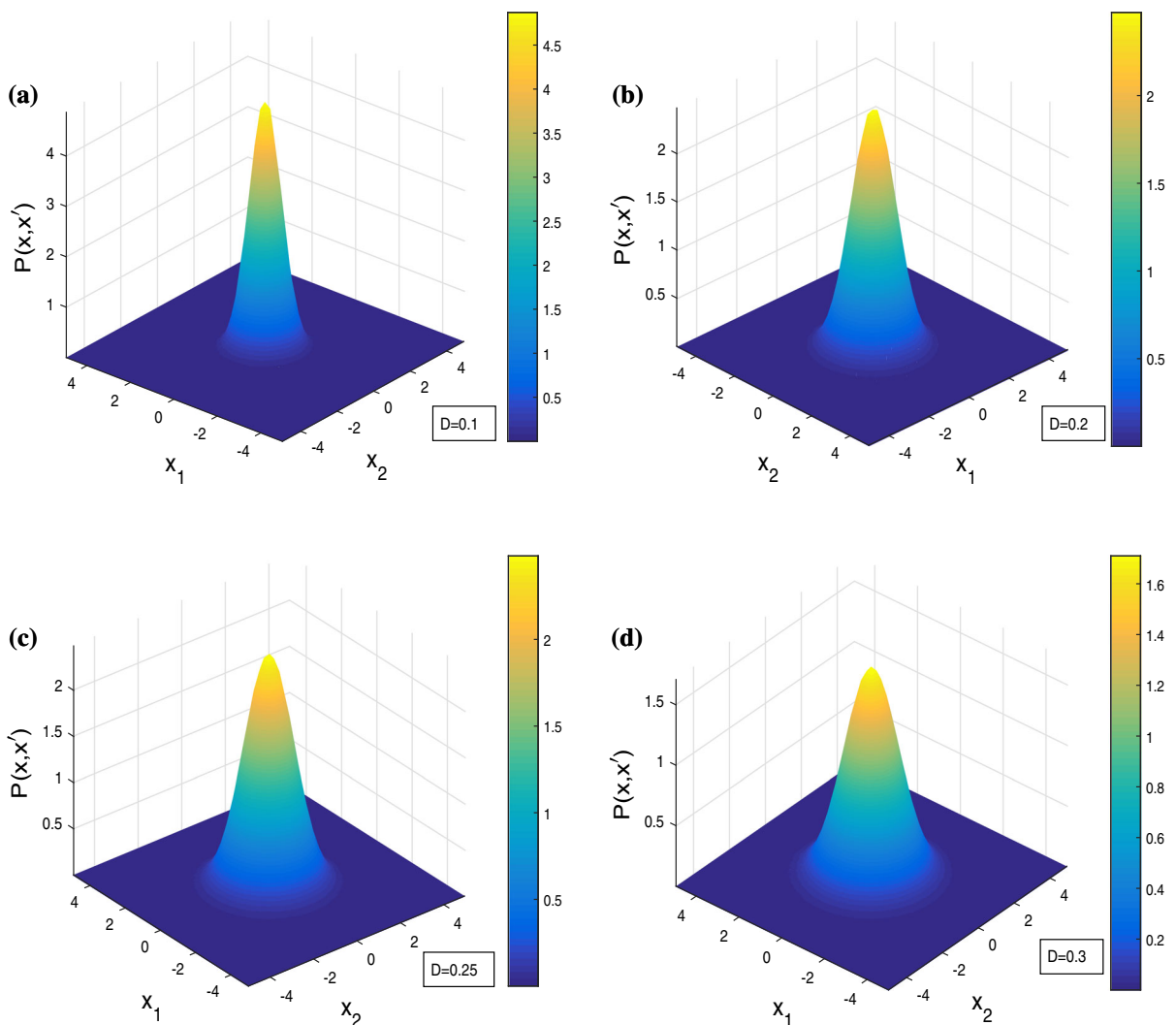


**Fig. 2** Stationary probability density of the system in 3D representation for: for  $\mu_a = 0.3$ ,  $\beta_2 = 0.005$ ,  $\beta_1 = 0.003$ ,  $\alpha_2 = 0.000001$ ,  $\beta_{22} = -0.005$ ,  $\beta_{11} = 0.003$ ,  $\alpha_3 = 0.0003$ ,  $\sigma = 0.05$ ,  $\omega_0 = 1$

**Fig. 3** **a** Evolution of mean square voltage of piezoelectric circuit versus coefficient  $\beta_{11}$ , **b** Evolution of mean square current of magnetic circuit versus coefficient  $\beta_{22}$  for  $\mu_a = 0.3$ ,  $\beta_2 = 0.005$ ,  $\beta_1 = 0.003$ ,  $\alpha_2 = 0.000001$ ,  $\beta_{22} = -0.005$ ,  $\beta_{11} = 0.003$ ,  $\alpha_3 = 0.0003$ ,  $\sigma = 0.05$ ,  $D = 0.1$ ,  $\omega_0 = 1$

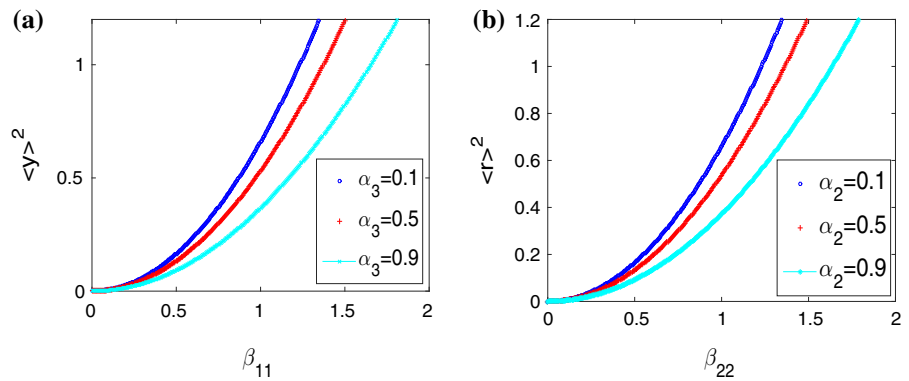
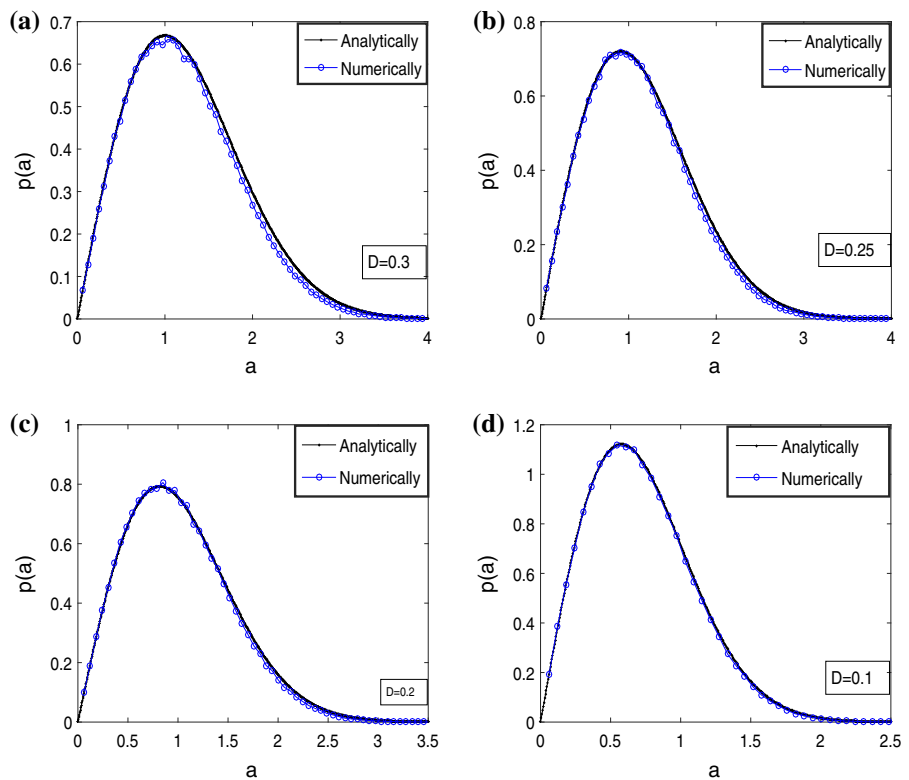


**Fig. 4** Stationary probability density for different values of noise intensity for  $\mu_a = 0.3$ ,  $\beta_2 = 0.005$ ,  $\beta_1 = 0.003$ ,  $\alpha_2 = 0.000001$ ,  $\beta_{22} = -0.005$ ,  $\beta_{11} = 0.003$ ,  $\alpha_3 = 0.0003$ ,  $\sigma = 0.05$ ,  $\omega_0 = 1$



mean response amplitude and phase lag respectively at the frequency  $j\omega_i$ . The mean amplitude response is defined as in Ref. [13]:

$$x_m = \sqrt{A_s^2 + A_c^2} \tag{21}$$

where  $A_s$  and  $A_c$  are the  $i$ th sine and cosine components of the Fourier coefficients defined as follows:

$$A_s = \frac{2}{nT} \int_0^{nT} x(\tau) \sin(\omega_i \tau) d\tau \tag{22}$$

$$A_c = \frac{2}{nT} \int_0^{nT} x(\tau) \cos(\omega_i \tau) d\tau$$

where  $n = 500$ , while  $T = \frac{2\pi}{\omega_i}$  is the period harmonic excitation.

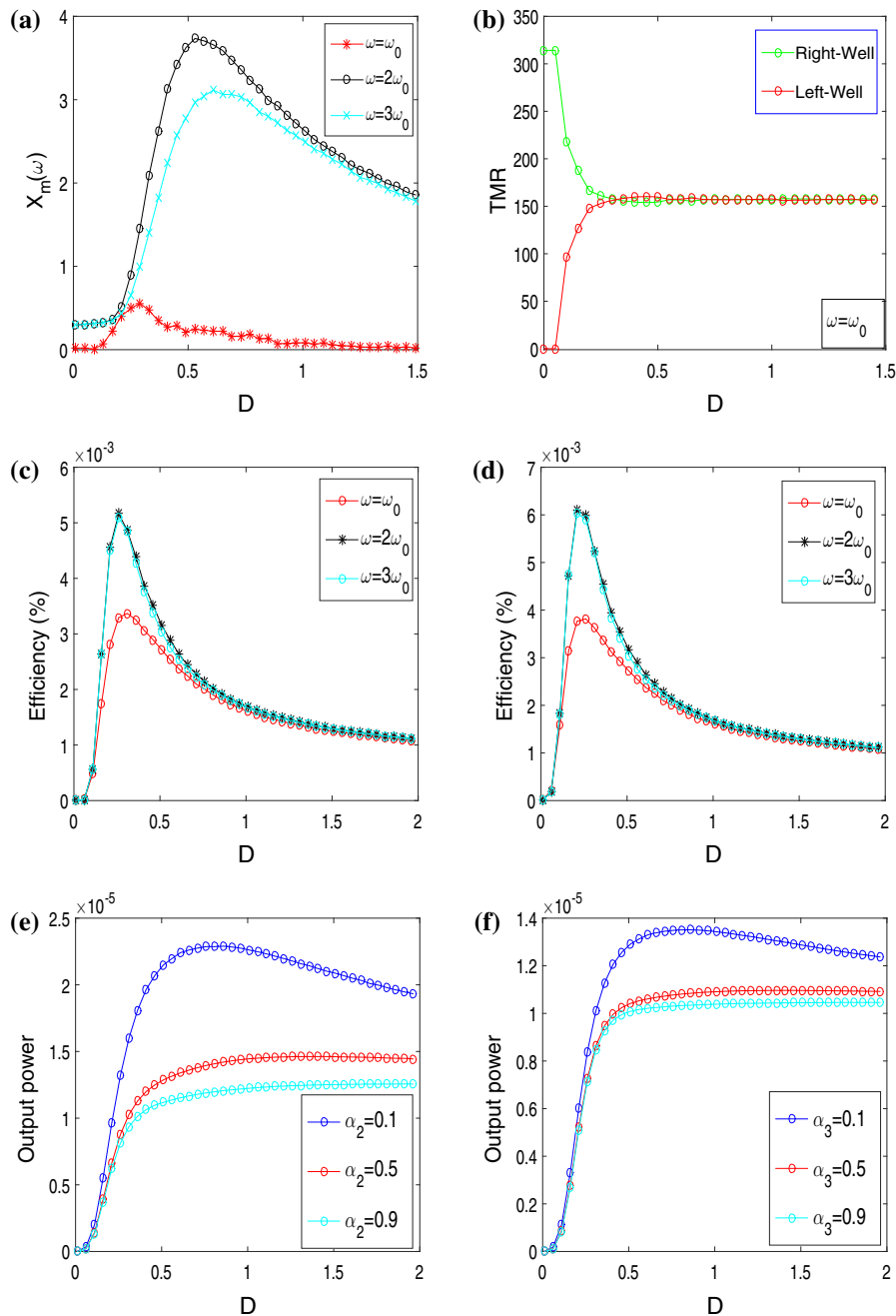


**Fig. 5** **a** Mean amplitude response  $x_m(\omega)$  versus noise intensity  $D$ , **b** Mean residence time versus noise intensity  $D$ , **c–d** Efficiency versus noise intensity  $D$  for

$\alpha_3 = 0.0003, \alpha_2 = 0.000001$ , **e–f** Output voltage versus noise intensity for  $\mu_a = 0.3, \beta_2 = 0.005, \beta_1 = 0.003, \beta_{22} = -0.005, \beta_{11} = 0.003, \sigma = 0.05, f_0 = 0.39, \omega_0 = 1$

Figure 5a shows the evolution of the numerically computed  $x_m(\omega)$  for  $\omega = \omega_0, \omega = \omega_1 = 2\omega_0$  and  $\omega = \omega_2 = 3\omega_0$  as a function of the noise intensity  $D$ . A typical noise-induced resonance is realized with these frequencies.  $\omega_1$  and  $\omega_2$  are present in the input signal.

The resonance observed with these frequencies is the usual stochastic resonance [24, 25]. The resonance associated with the missing frequency  $\omega_0$  is ghost-stochastic resonance. The ghost-stochastic resonance occurs at  $D = D_{max} = 0.3$ . This can be corroborated in



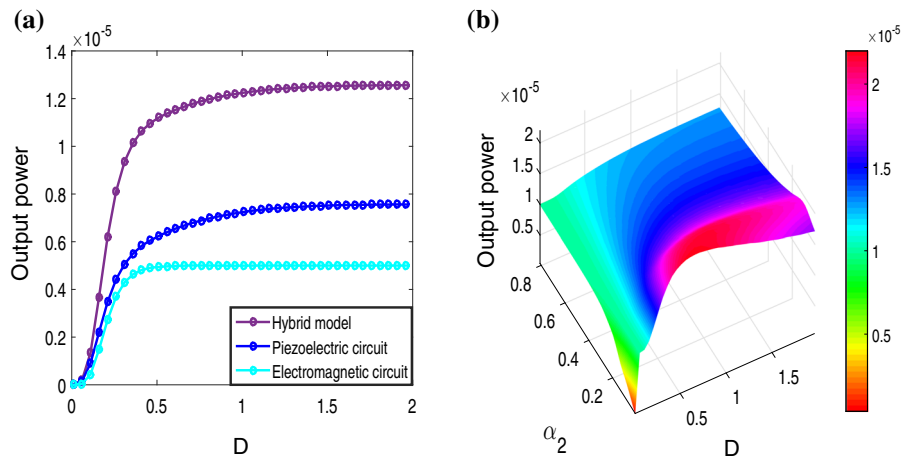


**Fig. 6** **a** Output power versus noise intensity D, **b** 3D-representation of the Output power of hybrid model versus noise intensity D and piezoelectric coupling coefficient for

$$\alpha_3 = 0.0003, \alpha_2 = 0.000001, \mu_a = 0.3, \beta_2 = 0.005, \beta_1 = 0.003, \beta_{22} = -0.005, \beta_{11} = 0.003, \sigma = 0.05, f_0 = 0.39, \omega_0 = 1$$

**Fig. 7** **a, c**, Time series of the mechanical subsystem, **b, d**, Probability distribution of the mechanical subsystem for  $\mu_a = 0.3, \beta_2 = 0.005, \beta_1 = 0.003, \alpha_2 = 0.000001, \beta_{22} = -0.005, \beta_{11} = 0.003, \alpha_3 = 0.0003, \sigma = 0.05, f_0 = 0.39, \omega_0 = 1$

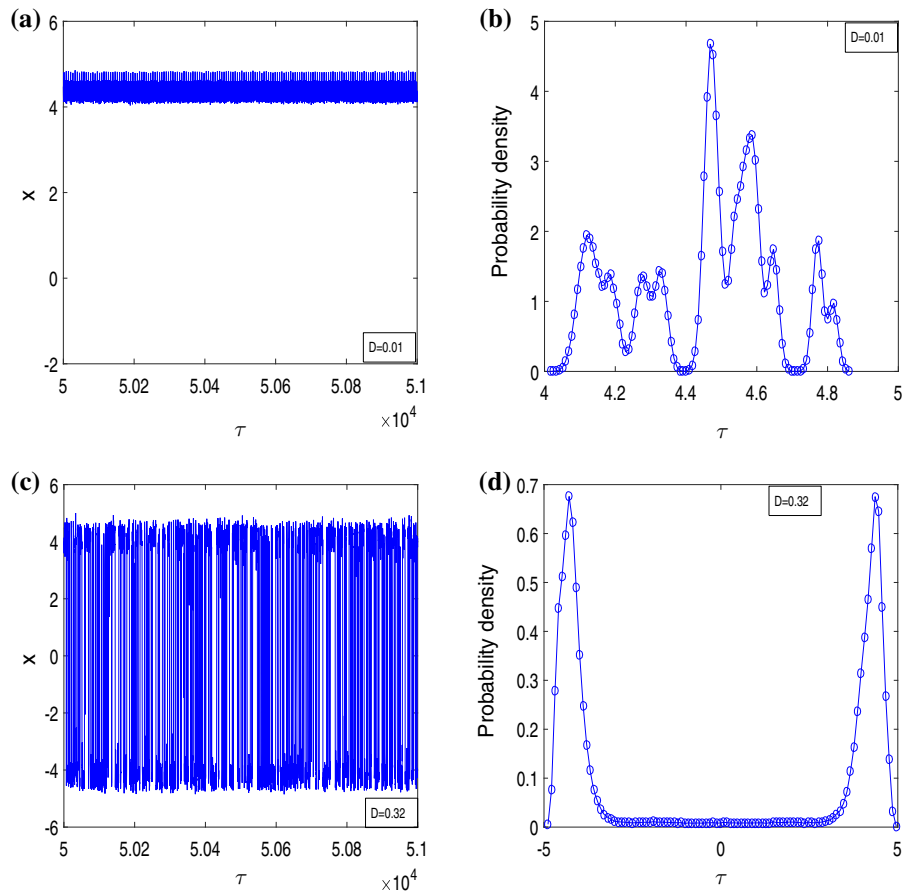
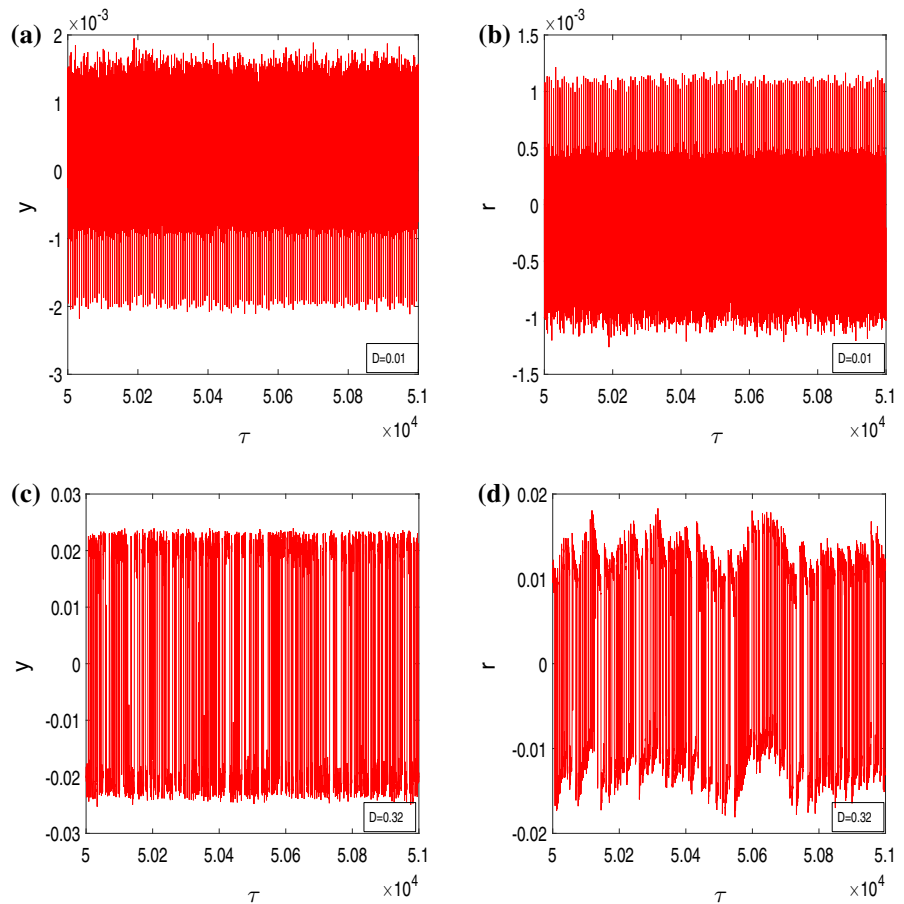


Fig. 5b by plotting the mean residence time. Indeed, in Fig. 5b, when the noise intensity D is equal to

$D = 0.05$ , the size of the orbit increases when the value of D increases. However, the orbit remains in the

**Fig. 8** Time series of the piezoelectric voltage and magnetic current, **a** Voltage of piezoelectric circuit before the ghost-stochastic resonance, **b** Magnetic current of the magnetic circuit before the ghost-stochastic resonance, **c** Voltage of piezoelectric circuit when the ghost-stochastic resonance occurs, **d** Magnetic current of the magnetic circuit when the ghost-stochastic resonance, for for  $\mu_a = 0.3$ ,  $\beta_2 = 0.005$ ,  $\beta_1 = 0.003$ ,  $\alpha_2 = 0.000001$ ,  $\beta_{22} = -0.005$ ,  $\beta_{11} = 0.003$ ,  $\alpha_3 = 0.0003$ ,  $\sigma = 0.05$ ,  $f_0 = 0.39$ ,  $\omega_0 = 1$



right well. For  $D \geq 0.05$ , the orbit visits the left well and gives rise to the ghost-stochastic resonance phenomenon when the noise intensity takes the value  $D = D_{max} = 0.3$ .

In Fig. 6a, we compare the output power generated by the hybrid model and those obtained by the piezoelectric and electromagnetic model respectively. We notice that the energy harvested by the hybrid model is higher than the one harvested by the piezoelectric or electromagnetic circuit. We provide in Fig. 6b, the 3D-representation of the output power of the hybrid model versus noise intensity and electrical impedance of piezoelectric circuit  $\alpha_2$ . We observe that, for a fixed value of noise intensity  $D$ , the maximum of output power decreases when  $\alpha_2$  increases.

### 4.3 Efficiency in power conversion of the harvester

The efficiency conversion of energies dispersed in the environment by the electricity’s generator is the one of the fundamental elements for evaluating the system’s performance. Thus, the efficiency of the hybrid model is assessed by using this formula:

$$\eta = \frac{P_e}{P_m} \times 100 \tag{23}$$

with  $P_e$  and  $P_m$ , are respectively, the electrical and the mechanical power effective value. It is well known in the literature that the power effective value is defined as:

$$p_t = \sqrt{\frac{1}{\tau} \int_0^\tau (p_t^{ins})^2 d\tau} \tag{24}$$

where  $p_t^{ins}$  is the instantaneous power and  $\tau$  is the time.

In Fig. 5c, d, we draw the efficiency conversion of the piezoelectric and electromagnetic subsystem versus noise intensity  $D$ . It emerges from these figures that, when  $\omega = \omega_0$ , the efficiency increases for  $D < D_{max}$ , reaches a maximum for  $D = D_{max} = 0.3$  when the ghost-stochastic resonance occurs, and decreases for  $D > D_{max}$ . We also provided in Fig. 5e, f, the output power for  $\omega = \omega_0$ , for different values of electrical impedance of the piezoelectric  $\alpha_2$  and magnetic circuit  $\alpha_3$ . We observe in these figures that, while the fundamental frequency is absent in the input signal, the harvester can generate a significant energy. In addition, we also notice in these figures Fig. 5e, f that, an enhancing the  $\alpha_2$  and  $\alpha_3$  lead to decrease the output power.

We plotted in Fig. 7, the time series of the harvester, with the corresponding probability distribution. In Fig. 7a, b, we observe that the system vibrates in the right-well and presents a lot of maximum and minimum. No any transition is observed in this condition. However, in Fig. 7c, the transition phenomenon is observed. The system vibrates around the position  $X = 0$  between the positions  $X = -4.29$  and  $X = 4.359$ . This is corroborated by Fig. 7d. We plot in Fig. 8a–d, the voltage of the piezoelectric subsystem and the magnetic current of the magnetic circuit versus the time, corresponding to the probability density function plotted in Fig. 7b, d. We notice in Fig. 8, the amplitude of the voltage of the piezoelectric circuit and magnetic current of the magnetic circuit is higher when the ghost-stochastic resonance occurs. Thus, when the ghost-stochastic resonance occurs, the piezoelectric output power and the magnetic output power will be maximized, and consequently, improves the amount of energy harvested by the scavenger. This shows the correlation between the peaks location in the probability density function and the output power.

## 5 Discussion

In a broad sense and as we show in this work, kinetic energy harvesters can convert any mechanical motion (like fluid flows, pressure variations and ambient vibrations) into electrical energy to power systems located in its environs [26]. In this purpose, it is

necessary to take account of the presence of nonlinearity, both desired and undesired. Nonlinearities appear through nonlinearity in the spring force [27] and others component's nonlinearities. A number of recent contributions seek to use nonlinearity in a novel way to improve the harvesters performances (see [28–30]), thus justifying the consideration of nonlinearity in this work.

This work shows that for our device, the maximum power of the hybrid model is greater than that of the piezoelectric and electromagnetic models independently (Fig. 6). As pointed in [31], hybridization of two conversion mechanisms in a single system improved the functionality of the harvester in the low frequency range (such as vehicle motion, human motion, and wave heave motion, which usually occur at low frequencies ( $< 20\text{Hz}$ ) [32–34]). It is seen that the results are qualitatively in rather good agreement with those from [35], that noticed that the total synergistically extracted power from the hybrid harvester is more than the power obtained from each independently. Many authors [36–38] have pointed that, hybridization could be deliberately exploited within a mechanical system for optimized energy harvesting. Experimental results from [35] confirms that the extracted power at various loading conditions for available ambient excitations is greater.

In this manuscript, the harmonic excitation is combined with Gaussian white noise. As we mentioned in the preceding sections, the type of energy harvester system under study, could be subjected to noise, coming from many sources (such as physical structure-generated noise [39], environmental and transportation noise [40–43] and pneumatic noise [44–46]).

The results obtained in this work, shows an improvement of the system performance when the noise intensity is around  $D \approx 0.3$  (See Fig. 5c, d) for a frequency of vibration absent in the frequency bandwidth of the harmonic force. It is known in the literature that, when the nonlinear system is subjected to the combination of the harmonic excitation and the random force, many phenomena can be observed such as the stochastic resonance and the ghost-stochastic resonance. These two phenomena are characterized by the large amplitude of vibration [47–49]. Zheng et al. [50, 51] in their work, have indicated that the available power generated under stochastic resonance is noticeably higher than the power that can be collected under

other harvesting conditions. As in this study this resonance occurs and the maximum amplitude of the system is reached for a frequency of vibration absent in the frequency bandwidth of the harmonic force, this phenomenon is called a ghost-stochastic resonance [52–55].

## 6 Conclusion

In summary, the hybrid energy scavenging device subjected to the Gaussian White noise is investigated. Using the stochastic averaging method, we constructed the *Fokker – Plank – Kolmogorov* equation whose the solution in the stationary state is the probability density. From this statistic response, we assessed the output power of the piezoelectric and electromagnetic circuit under the form of mean square voltage and current. The impact of electrical impedance of piezoelectric and electromagnetic subsystem is presented with detail. It emerges from these results that, the output power of the two electrical circuit enhance when the coupling parameters increase while a enhancing of the electrical impedances lead to the reduction of the output power. In addition, combining the coherence force with random excitation, the ghost-stochastic resonance occur and improved the system performance. The agreement between the analytical and numerical results validated the efficiency of the analytical method proposed. The results obtained in this manuscript reveal that, while the natural frequency is absent in the coherent excitation, the system performance can be improved for certain value of the noise intensity.

### Compliance with ethical standards

**Conflict of interest** The authors declare that they have no conflict of interest.

## References

- Mitcheson PD, Miao P, Stark BH, Yeatman EM, Holmes AS, Green TC (2004) MEMS electrostatic micropower generator for low frequency operation. *Sens Actuators, A* 115:523
- Sari I, Balkan T, Kulah H (2008) An electromagnetic micro power generator for wideband environmental vibrations. *Sens Actuators, A* 145:405
- Buckjohn CND, Martin SS, Mokem Fokou IS, Tchawoua C, Kofane TC (2013) Investigating bifurcations and chaos in magnetopiezoelectric vibrating energy harvesters using Melnikov theory. *Phys Scr* 88:015006
- Elvin N, Erturk A (2013) *Advances in energy harvesting methods*. Springer, New York
- Daqaq MF, Masana R, Erturk A, Quinn DD (2014) On the role of nonlinearities in vibratory energy harvesting: a critical review and discussion. *Appl Mech Rev* 66:040801
- Mann BP, Owens BA (2010) Investigations of a nonlinear energy harvester with a bistable potential well. *J Sound Vib* 329:1215–1226
- Elvin NG, Elvin AA, Spector M (2001) A self-powered mechanical strain energy sensor. *Smart Mater Struct* 10(2):293–299
- Kim HW, Priya S, Uchino K, Newnham RE (2005) Piezoelectric energy harvesting under high pre-stressed cyclic vibrations. *J Electroceramics* 15(1):27–34
- Lee B, Wei L (2010) Hybrid energy harvester based on piezoelectric and electromagnetic mechanisms. *J Micro/Nanolith MEMS MOEMS* 9(Apr–Jun (2)):023002
- Wang C, Yanlong C, Jin X (2015) Piezoelectric and electromagnetic hybrid energy harvester for powering wireless sensor nodes in smart grid. *J Mech Sci Technol* 29:4313
- Madinei H, Haddad KH, Adhikari S, Friswell MI (2016) A hybrid piezoelectric and electrostatic vibration energy harvester. In: Brandt A, Singhal R, (eds), *Shock, vibration, aircraft/aerospace, energy harvesting acoustics optics*, vol 9 pp 189–95
- Cottone F, Vocca H, Gammaitoni L (2009) Nonlinear energy harvesting. *Phys Rev Lett* 102:08060
- Mokem Fokou IS, Nono Dueyou Buckjohn C, Siewe Siewe M, Tchawoua C (2016) Probabilistic behavior analysis of a sandwiched buckled beam under Gaussian white noise with energy harvesting perspectives. *Chaos, Solitons Fractals* 92:101–114
- Fokou ISM, Buckjohn CND, Siewe MS, Tchawoua C (2018) Probabilistic distribution and stochastic P-bifurcation of a hybrid energy harvester under colored noise. *Commun. Nonlinear Sci Numer Simulat* 56:177–197
- Foupouapouognigni O, Nono Dueyou Buckjohn C, Siewe Siewe M, Tchawoua C (2018) Hybrid electromagnetic and piezoelectric vibration energy harvester with Gaussian white noise excitation. *Physica A Stat Mech Appl* 509:346–360
- Berthet R, Petrosyan A, Roman B (2002) *Am J Phys* 70:744
- Rowland DR (2004) *Am J Phys* 72:758
- Chialvo DR, Calvo O, Gonzalez DL, Piro O, Savino GV (2002) *Phys Rev E* 65:050902(R)
- Chialvo DR (2003) *Chaos* 13:1226
- Buldu JM, Chialvo DR, Mirasso CR, Torrent MC, Garcia-Ojalvo J (2003) *Europhys Lett* 64:178
- Buldu JM, Gonzalez CM, Trull J, Torrent MC, Garcia-Ojalvo J (2005) *Chaos* 15:013103
- Van der Sande G, Verschaffelt G, Danckaert J, Mirasso CR (2005) *Phys Rev E* 72:016113
- Lefeuvre E, Badel A, Richard C, Petit L, Guyomar D (2006) A comparison between several vibration-powered piezoelectric generators for standalone systems. *Sens Actuators A* 126(2):405–416

24. Mokem Fokou IS, Nono Dueyou Buckjohn C, Siewe Siewe M, Tchawoua C (2017) Nonlinear analysis and analog simulation of a piezoelectric buckled beam with fractional derivative. *Eur Phys J Plus* 132:344
25. Mokem Fokou IS, Nono Dueyou Buckjohn C, Siewe Siewe M, Tchawoua C (2018) Circuit implementation of a piezoelectric buckled beam and its response under fractional components considerations. *Meccanica* 53(8):2029–2052
26. Knight C, Davidson J, Behrens S (2008) Energy options for wireless sensor nodes. *Sensors* 8(12):8037–8066
27. Miki D, Honzumi M, Suzuki Y, Kasagi N (2010). Large-amplitude mems electret generator with nonlinear spring. In: *Proceedings of IEEE conference on microelectromechanical systems (MEMS) 2010*, 24–28 January 2010, Wanchai, Hong Kong, (pp. 176–179)
28. Yanxia Z, Yanfei J, Pengfei X, Shaomin X (2020) Stochastic bifurcations in a nonlinear tri-stable energy harvester under coloured noise. *Nonlinear Dyn* 99:879–897
29. Constantinou P, Roy S (2016) A 3D printed electromagnetic nonlinear vibration energy harvester. *Smart Mater Struct* 25(9):095053 (1–14)
30. Junlei W, Linfeng G, Shengxi Z, Zhien Z, Zhihui L, Daniil Y (2020) Design, modelling and experiments of broadband tristable galloping piezoelectric energy harvester. *Acta Mechanica Sinica*. <https://doi.org/10.1007/s10409-020-00928-5>
31. Toyabur RM, Salaudiddin M, Hyunok C, Park Jae Y (2018) A multimodal hybrid energy harvester based on piezoelectric-electromagnetic mechanisms for low-frequency ambient vibrations. *Energy Convers Manage* 168:454–466
32. Fan KQ, Chang JW, Pedrycz W, Liu ZH, Zhu YM (2015) A nonlinear piezoelectric energy harvester for various mechanical motions. *Appl Phys Lett* 106:223902
33. Tang LH, Yang YW, Soh CK (2012) Improving functionality of vibration energy harvesters using magnets. *J Intell Mater Syst Struct* 23:1433–49
34. Fan KQ, Chang JW, Chao FB, Pedrycz W (2015) Design and development of a multipurpose piezoelectric energy harvester. *Energy Convers Manage* 96:430–39
35. Salar C, Hasan U, Ali M, Berkay C, Haluk K (2015) Power-efficient hybrid energy harvesting system for harnessing ambient vibrations. *IEEE Trans Circuits Syst I Regul Pap* 66(7):2784–2793 2019
36. Kangqi F, Qinxue T, Haiyan L, Daxing Z, Yingmin Z, Weidong W (2018) Hybrid piezoelectric-electromagnetic energy harvester for scavenging energy from low-frequency excitations. *Smart Mater Struct* 27(8):085001
37. Mahmoudi S, Kacem N, Bouhaddi N (2014) Enhancement of the performance of a hybrid nonlinear vibration energy harvester based on piezoelectric and electromagnetic transductions. *Smart Mater Struct* 23:075024
38. Xia H, Chen R, Ren L (2015) Analysis of piezoelectric—electromagnetic hybrid vibration energy harvester under different electrical boundary conditions. *Sens Actuators A* 234:87–98
39. Aylin T (2018) Noise Reduction Techniques for Medical Equipment Manufacturers, *Advancements in Noise Reduction Techniques for Medical Equipment Manufacturers*, Parker Hannifin Corporation
40. Dzhambov Angel M, Dimitrova Donka D (2016) Heart disease attributed to occupational noise, vibration and other co-exposure: self-reported population-based survey among Bulgarian workers. *Med Pr* 67(4):435–445
41. Ilona C, Michael GS, Kerstin PW (2013) Effects of train noise and vibration on human heart rate during sleep: an experimental study. *BMJ Open* 3(5):e002655
42. Tassi P, Saremi M, Schimchowitsch S, Eschenlauer A, Rohmer O, Muzet A (2010) *Eur J Appl Physiol* 108:671–680
43. Sandra P, De Elke V, Raymond C (2010) Nocturnal road traffic noise: a review on its assessment and consequences on sleep and health. *Environ Int* 36:492–498
44. Joseph G (1960) Gallop rhythm of the heart: I atrial gallop, ventricular gallop and systolic sounds. *Am J Med* 28(4):578–592
45. Schmidt SE, Graebe M, Toft E, Struijk JJ (2011) No evidence of nonlinear or chaotic behaviour of cardiovascular murmurs. *Biomed Signal Process Control* 6(2):157–163
46. Thomas SL, Makaryus AN (2020) Physiology, cardiovascular murmurs. [Updated 2019 Jun 3]. In: *Stat Pearls* [Internet]. Treasure Island (FL): Stat Pearls Publishing. Available from: <https://www.ncbi.nlm.nih.gov/books/NBK525958>
47. Mantegna RN, Spagnolo B, Testa L, Trapanese M (2005) Stochastic resonance in magnetic systems described by Preisach hysteresis model. *J Appl Phys* 97:223–87
48. Arathi S, Rajasekar S, Kurths J (2011) Characteristics of stochastic resonance in asymmetric dufing oscillator. *Int J Bifurcation Chaos* 21:2729
49. Gammaitoni L, Hanggi P, Jung P, Marchesoni F (1998) Stochastic resonance. *Rev Mod Phys* 70:223–87. <https://doi.org/10.1103/RevModPhys.70.223>
50. Zheng R, Nakano K, Hu H, Su D, Cartmell MP (2014) An application of stochastic resonance for energy harvesting in a bistable vibrating system. *J Sound Vib* 333:2568–87
51. Hu H, Nakano K, Cartmell M, Zheng R, Ohori M (2012) An experimental study of stochastic resonance in a bistable mechanical system. *J Phys* 382:012024 (1–6)
52. Buldu JM, Chialvo DR, Mirasso CR, Torrent MC, Garcia-Ojalvo J (2003) Ghost resonance in a semiconductor laser with optical feedback. *Europhys Lett* 64:178
53. Buldu JM, Gonzalez CM, Trull J, Torrent MC, Garcia-Ojalvo J (2005) Coupling-mediated ghost resonance in mutually injected lasers. *Chaos* 15:013103
54. Van der Sande G, Verschaffelt G, Danckaert J, Mirasso CR (2005) Ghost stochastic resonance in vertical-cavity surface-emitting lasers: experiment and theory. *Phys Rev E* 72:016113
55. Lopera A, Buldu JM, Torrent MC, Chialvo DR, Garcia-Ojalvo J (2006) Ghost stochastic resonance with distributed inputs in pulse-coupled electronic neurons. *Phys Rev E* 73:021101

**Publisher's Note** Springer Nature remains neutral with regard to jurisdictional claims in published maps and institutional affiliations.